Time Domain and Frequency Domain Induced Polarization Modeling for Three-dimensional Anisotropic Medium

Weiqiang Liu[1], Pinrong Lin[1], Qingtian Lü[1], Rujun Chen[2], Hongzhu Cai[3] and Jianhua Li[1]
[1]Institute of Geophysical and Geochemical Exploration of Chinese Academy of Geological Sciences and Laboratory of Geophysical EM Probing Technologies, MLR, Langfang, P.R. China
[2]Central South University, School of Geoscience & Info-Physics, Changsha, P.R. China
[3]University of Utah, Consortium for Electromagnetic Modeling and Inversion (CEMI), Salt Lake City, Utah, USA

ABSTRACT

Time domain induced polarization (TDIP) and frequency domain induced polarization (FDIP) synthetic models, incorporating three-dimensional (3D) anisotropic medium, were tested. In TDIP modeling, both resistivity and chargeability of the medium were anisotropic, and the apparent chargeability values were calculated by carrying out two resistivity forward calculations using resistivity with and without an IP effect. We analyzed the TDIP response of a 3D isotropic cube model embedded in the anisotropic subsurface half-space. In FDIP modeling, the complex resistivity of the medium at various frequencies was anisotropic. The complex resistivity was determined by a Cole-Cole model with anisotropic model parameters. We then analyzed the FDIP response of a 3D anisotropic cube model embedded in an isotropic subsurface half-space. Both of the TDIP and FDIP simulation results suggest that IP responses acquired in two orthogonal directions on the surface are different when the same arrays are used and acquisition in orthogonal directions helps resolve the presence of anisotropy. The anisotropy should be taken into account in practice for TDIP and FDIP exploration.

Introduction

Induced polarization (IP) responses are directly proportional to the volume content of metallic grains, which is a good indicator for the presence of ore bodies (Revil *et al*., 2015a, b). Compared with the conventional direct current (DC) resistivity method, IP methods operated in both the time domain and the frequency domain are effective in exploration for nonferrous metallic deposits (Sastry and Tesfakiros, 2006; Schmutz *et al*., 2011; Marchant *et al*., 2014; Loke *et al*., 2014; Liu *et al*., 2016; Liu *et al*., 2017). Most often, it is assumed that these deposits are comprised of an isotropic medium. In practical prospecting, however, the earth medium shows anisotropic electrical effects caused by tilted stratified rocks, parallel or vertical fracturing, specific mineral crystals, and inhomogeneous sedimentation rates (Wang *et al*., 2013).

Over the past several years, there has been significant development in 3D distributed IP acquisition systems to reduce field time and to increase spatial coverage (Chen *et al*., 2010; Sun *et al*., 2012; Gharibi *et al*., 2012; McGill and Farquhar-Smith, 2015). In practical field surveys now, IP data of each survey station can be acquired in orthogonal directions easily, which are necessary to characterize anisotropic IP effects. Many experts have studied forward modeling algorithms of anisotropic DC resistivity (Yin, 2000; Li and Spitzer, 2005; Wang *et al*., 2013), however, only a few scholars have studied the anisotropic induced polarization modeling. Zhdanov *et al*. (2008) developed a new generalized effective-medium theory of induced polarization (GEMTIP) to model complex resistivity and studied the anisotropy effect in IP data. Winchen *et al*. (2009) investigated anisotropic complex conductivity of the two isotropic materials with heterogeneous mixtures, and the Cole-Cole model was used to depict soil with bimodal textural characteristics. Kenkel *et al*. (2012) discussed mixing laws for anisotropic complex conductivity in layered situations, and employed a 2.5 D finite element method to model and inverse the anisotropic complex conductivity response.

Although there is a rich historical set of papers that have covered many aspects of anisotropy in electrical media, none have specifically investigated the issue for both TDIP and FDIP. Therefore, in this work we conduct

 DOI: #10.2113/JEEG22.4.435

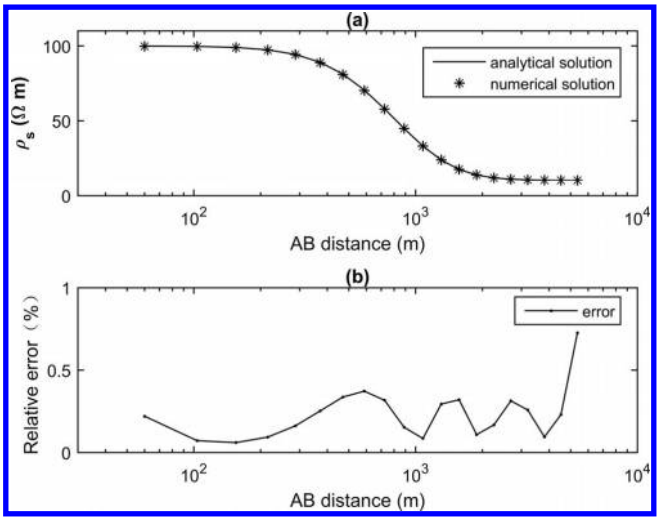

Figure 1. Apparent resistivity curve using Schlumberger sounding arrangement for a two-layer vertical anisotropic model: a) analytical solution and numerical solution; b) the relative error.

numerical modeling of 3D anisotropic bodies with TDIP and FDIP with different arrangements of isotropic or anisotropic earth. One of the major conclusions from this study is that ignoring anisotropy may yield misleading results.

3D Anisotropic TDIP Modeling

In TDIP forward modeling, the resistivity ($\boldsymbol{\rho}$) and chargeability ($\boldsymbol{\eta}$) of the earth medium are anisotropic, which can be expressed as a tensor:

$$\boldsymbol{\rho} = \begin{pmatrix} \rho_{xx} & 0 & 0 \\ 0 & \rho_{yy} & 0 \\ 0 & 0 & \rho_{zz} \end{pmatrix} \qquad \boldsymbol{\eta} = \begin{pmatrix} \eta_{xx} & 0 & 0 \\ 0 & \eta_{yy} & 0 \\ 0 & 0 & \eta_{zz} \end{pmatrix} \tag{1}$$

When the medium is chargeable, the resistivity of the medium with an IP effect is $\boldsymbol{\rho}[1-\boldsymbol{\eta}]^{-1}$, and the governing equation and boundary conditions of the potential for the anisotropic electrical model in direct current field can be expressed as:

$$\begin{cases} \nabla \bullet \left(\dfrac{1}{\boldsymbol{\rho}}(1-\boldsymbol{\eta})\nabla U\right) = -I\delta(\mathbf{r}-\mathbf{r}_q) \\ \dfrac{\partial U}{\partial n} = 0 & \in \Gamma_S \\ \dfrac{1}{\boldsymbol{\rho}}(1-\boldsymbol{\eta})\dfrac{\partial U}{\partial n} + \dfrac{|\mathbf{r}-\mathbf{r}_q|\cos(\mathbf{r},\mathbf{n})}{B}U = 0 & \in \Gamma_\infty \end{cases} \tag{2}$$

where $\mathbf{r}$ and $\mathbf{r}_q$ are locations of the potential electrode and the point current source. $(1/\boldsymbol{\rho})(1-\boldsymbol{\eta})$ is the chargeable conductivity tensor, and B is the equivalent distance calculated using $\mathbf{r}$, $\mathbf{r}_q$ and $(1/\boldsymbol{\rho})(1-\boldsymbol{\eta})$. A Neumann boundary condition is at the earth and air interface Γs, and a mixed boundary condition is on the infinite boundary Γ_∞. Further, we used $\boldsymbol{\rho}$ and the chargeable resistivity $\boldsymbol{\rho}[1-\boldsymbol{\eta}]^{-1}$ to calculate the primary voltage U and the total voltage U_t through solving Laplace equation, respectively.

The finite volume method (FVM) was used to approximate this anisotropic boundary value problem. The model is subdivided into a number of small cell-centered hexahedron volumes surrounding each node point. For each volume, the partial derivative is replaced by the difference of the potential in corresponding two boundaries according to Gaussian divergence theorem (Haber *et al.*, 2000). After approximating the governing equation in all the volumes and assembling them into a large matrix, a linear system of equations is obtained. In this work, the linear set was solved by the Intel MKL PARDISO solver. Finally, apparent chargeability can be calculated using the surface primary voltage and the total voltage (Oldenburg and Li, 1994).

To verify the accuracy of the FVM method, we used a two-layer vertical anisotropic resistivity model. The first layer is 100 m thick and the tensoral resistivity is $\boldsymbol{\rho} = \begin{pmatrix} 50 & 0 & 0 \\ 0 & 50 & 0 \\ 0 & 0 & 200 \end{pmatrix}$ ohm-m. The second layer is homogeneous half space with $\boldsymbol{\rho} = 10$ ohm-m. A Schlumberger sounding arrangement was used with potential electrodes at a separation for MN = 20 m, and the current electrodes AB ranged from 60 m to 6,000 m. This two-layer vertical anisotropic model has an analytic solution to compare with our numerical results. (Wang *et al.*, 2013). Figure 1 shows the results of analytic solution and numerical solution with a relative error. The results from this two-layer model shows the mean error between the numerical and analytical was about 0.23% and max error was about 0.73%.

The second test was to determine the TDIP response of a 3D isotropic cube embedded in an anisotropic half-space with resistivity and chargeability as $\boldsymbol{\rho} = \begin{pmatrix} 120 & 0 & 0 \\ 0 & 480 & 0 \\ 0 & 0 & 120 \end{pmatrix}$ ohm-m and $\boldsymbol{\eta} = \begin{pmatrix} 0.15 & 0 & 0 \\ 0 & 0.05 & 0 \\ 0 & 0 & 0.15 \end{pmatrix}$, respectively. The isotropic 3D cube was 900 m × 900 m × 200 m with $\boldsymbol{\rho} = 10$ ohm-m and $\boldsymbol{\eta} = 0.3$. Depth of the cube center was 300 m. We simulated the apparent resistivity and apparent charge-

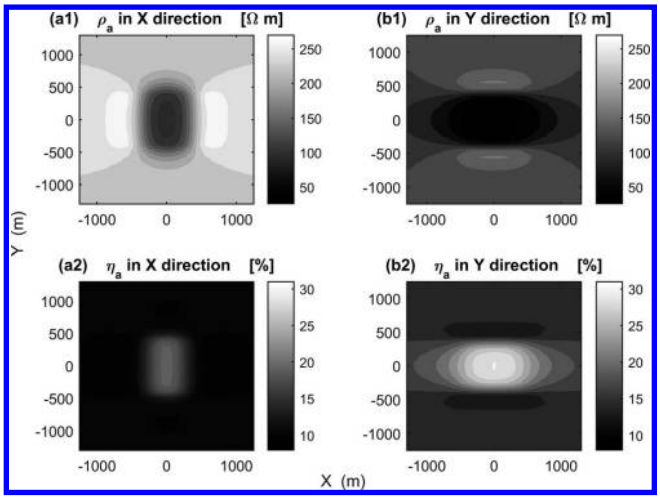

Figure 2. Simulated TDIP responses of an isotropic cube embed in an anisotropic half-space using two sets of orthogonal survey lines: a1) contour maps of apparent resistivity and a2) apparent chargeability when the survey lines are in X direction; b1) contour maps of apparent resistivity and b2) apparent chargeability when the survey lines are in Y direction.

ability responses at the surface in two separate orthogonal directions along the X and Y axes using the same arrays. We measured along 27 survey lines with 27 survey points per line in the X direction. Both electrode distance and line distance were 100 m. The total length of each survey line was 2,600 m. The intermediate gradient array protocol was used with current electrode separation of AB = 3,800 m and potential electrode space MN = 100 m. Second, the same survey lines and array protocol were conducted in the orthogonal direction along the Y axis. Figure 2 shows contour maps of the apparent resistivity and apparent chargeability when survey lines are along X direction and Y direction separately.

From Fig. 2, we see that the contour maps of the apparent resistivity and chargeability are different between X direction and Y direction. Near the border, apparent resistivity ${\rho_x}^a$ measured in X direction trends to $\sqrt{\rho_x \rho_y}$, and apparent ${\rho_y}^a$ measured in Y direction trends to ρ_x. This is the anisotropic paradox mentioned by Wang *et al*. (2013). The anisotropic phenomenon also exists in the IP response, with apparent chargeability ${\eta_x}^a$ trending to $1-\sqrt{(1-\eta_x)(1-\eta_y)}$ and ${\eta_a}^y$ trending to η_x.

3D Anisotropic FDIP Modeling

In the FDIP modeling, the amplitude and phase of the multi-frequency, complex resistivity was calculated by the Cole-Cole relaxation model with four parameters: resistivity ($\boldsymbol{\rho}_0$), chargeability ($\mathbf{m}$), time constant (τ) and a frequency dependent coefficient (c) (Pelton *et al*., 1978). When the medium is anisotropic, $\boldsymbol{\rho}_0$ and $\mathbf{m}$ are anisotropic, so complex resistivity of the anisotropic medium at frequency ω can be calculated as:

$$\boldsymbol{\rho}(\omega) = \boldsymbol{\rho}_0 * \left\{ 1 - \mathbf{m} * \left[1 - \frac{1}{\left(1 + (\mathrm{j}\omega\tau)^c\right)} \right] \right\} \qquad (4)$$

where $\boldsymbol{\rho}_0$ and $\mathbf{m}$ are tensors, τ and c are scalars. The electromagnetic coupling is a kind of electromagnetic interference in FDIP. When the alternating current is at a low frequency (about $10^{-3} \sim 1$ Hz), this coupling can be ignored, and one Cole-Cole model is enough to calculate the complex resistivity. However, when the frequency is high (about $1 \sim 10^3$ Hz), another Cole-Cole model with different parameters is also needed to fit the electromagnetic coupling. In this paper, only one model is used. Calculation of multi-model is similar to this. The anisotropic complex resistivity $\boldsymbol{\rho}(\omega)$ is substituted into the Laplace equation:

$$\begin{cases} \nabla \bullet \left(\dfrac{1}{\boldsymbol{\rho}(\omega)} \nabla U \right) = -I\delta(\mathbf{r} - \mathbf{r}_q) & \\ \dfrac{\partial U}{\partial n} = 0 & \in \Gamma_S \\ \dfrac{1}{\boldsymbol{\rho}(\omega)} \dfrac{\partial U}{\partial n} + \dfrac{|\mathbf{r} - \mathbf{r}_q| \cos(\mathbf{r}, \mathbf{n})}{B} U = 0 & \in \Gamma_\infty \end{cases} \qquad (5)$$

This boundary value problem is similar to that of TDIP with the sole difference being the resistivity parameter, which is complex (real and imaginary components) in FDIP and real in TDIP. The FDIP equation was also solved using FVM and the potential was obtained by solving a complex set of linear equations. From these equations and electrode arrangements, apparent resistivity and phase were calculated.

The FDIP response of a 3D anisotropic cube model embedded in the isotropic half-space was studied. The Cole-Cole model parameters of the isotropic half-space were $\boldsymbol{\rho} = 100$ ohm-m, $\mathbf{m} = 0.2$, $\tau = 1$ and $c = 0.25$. The anisotropic 3D cube was 900 m $\times$ 900 m $\times$ 200 m with $\boldsymbol{\rho} = \begin{pmatrix} 300 & 0 & 0 \\ 0 & 50 & 0 \\ 0 & 0 & 300 \end{pmatrix}$ ohm-m, $\mathbf{m} = \begin{pmatrix} 0.5 & 0 & 0 \\ 0 & 0.1 & 0 \\ 0 & 0 & 0.5 \end{pmatrix}$, $\tau = 1$ and $c = 0.25$. Depth of the cube center was 300 m. The frequency of the exciting current was 1 Hz. The survey lines and array protocol was the same as that in TDIP.

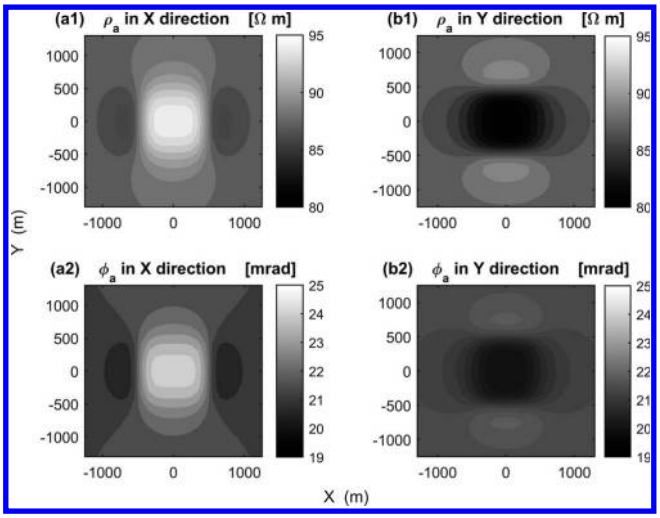

Figure 3. Simulated FDIP responses of an isotropic cube embed in an anisotropic half-space using two sets of orthogonal survey lines: a1) contour maps of apparent resistivity and a2) apparent phase when the survey lines are in X direction; b1) contour maps of apparent resistivity and b2) apparent phase when the survey lines are in Y direction.

We calculated the apparent resistivity and apparent phase responses in two orthogonal directions X and Y on the surface separately using the same arrays. Figure 3 shows contour maps of the apparent resistivity and apparent phase when survey lines are either along X or Y directions. From Figs. 3(a1) and 3(a2), there is a high resistivity and a high phase anomaly (relative to the background) in the center of the survey area when the survey lines are in the X direction. However, from Figs. 3(b1) and 3(b2), there is a low-resistivity and low-phase anomaly when the survey lines are in the Y direction. So the apparent parameters responses are different because of the anisotropy. Carbonaceous slate is a typical anisotropic body according to the rock samples measurements in our laboratory. Both resistivity and phase of this body measured perpendicular to the direction of the bedding may be 7∼10 times more than those measured parallel to the direction. In practical exploration, IP data should be acquired in two orthogonal directions to avoid misleading results caused by data only acquired in a single direction.

Conclusion and Discussion

In this paper, we conducted the 3D anisotropic TDIP and FDIP modeling using the finite volume method. Our work shows that both TDIP and FDIP apparent resistivity and apparent chargeability at the surface are related to the survey direction. In some cases, the IP anomalies measured at the surface in two directions may be opposite relative to the background (*i.e.,* more resistive or more conductive). Therefore, we believe that anisotropy should be taken into account in practical TDIP and FDIP exploration to ensure proper target definition. To rectify the anisotropy, we recommend that IP data be measured in two orthogonal directions to avoid misleading results. Additionally, although a meaningful forward algorithm is managed in this paper, there is still an urgent need to establish an inversion method to back calculate the anisotropic ratio in the further research.

Acknowledgments

This work was originally presented at SAGEEP 2017 and subsequently reformatted for submission to the Journal of Environmental and Engineering Geophysics as a Near Surface Geophysical Letter.

This research was sponsored by National Natural Science Foundation of China under grant (No. 41630320), Foundational and public welfare geology and mineral resources survey of China special project (No. DD20160046), National High Technology Research and Development Program of China (863 Program) (No. 2014AA06A610, 2014AA06A613), and the special funding of fundamental research of the Chinese Academy of Geological Sciences (YYWF201632).

References

Chen, R.J., He, Z.X., Qiu, J.T., He, L.F., and Cai, Z.X., 2010, Distributed data acquisition unit based on GPS and ZigBee for electromagnetic exploration: *in* Expanded Abstracts: Instrumentation and Measurement Technology Conference (I2MTC), IEEE, 981–985.

Gharibi, M., Killin, K., McGill, D., Henderson, W.B., and Retallick, T., 2012, Full 3D acquisition and modelling with the Quantec 3D system-the Hidden Hill Deposit case study: *in* Expanded Abstracts: 22nd International Geophysical Conference and Exhibition, The Australian Society of Exploration Geophysics (ASEG).

Haber, E., Ascher, U.M., Aruliah, D.A., and Oldenburg, D.W., 2000, Fast simulation of 3D electromagnetic problems using potentials: Journal of Computational Physics, **163**, 150–171.

Kenkel, J., Hördt, A., and Kemna, A., 2012, 2D modelling of induced polarization data with anisotropic complex conductivities: Near Surface Geophysics, **10**, 533–544.

Li, Y., and Spitzer, K., 2005. Finite element resistivity modelling for three-dimensional structures with arbitrary anisotropy: Physics of the Earth and Planetary Interiors, **150**, 15–27.

Liu, W., Chen, R., Cai, H., and Luo, W., 2016, Robust statistical methods for impulse noise suppressing of spread Spectrum induced polarization data, with application to a mine site,

Gansu Province, China: Journal of Applied Geophysics, **135**, 397–407.

Liu, W., Chen, R., Cai, H., Luo, W., and Revil, A., 2017, Correlation analysis for spread spectrum induced polarization signal processing in electromagnetically noisy environments: Geophysics, **82**, 1–48.

Loke, M.H., Dahlin, T., and Rucker, D.F., 2014, Smoothness-constrained time-lapse inversion of data from 3D resistivity surveys: Near Surface Geophysics, **12**, 5–24.

Marchant, D., Haber, E., and Oldenburg, D.W., 2014, Three-dimensional modeling of IP effects in time-domain electromagnetic data: Geophysics, **79**, E303–E314.

McGill, D., and Farquhar-Smith, D., 2015, A comparison of 3D DCIP data acquisition methods: *in* Expanded Abstracts: 24th International Geophysical Conference and Exhibition, The Australian Society of Exploration Geophysics (ASEG).

Oldenburg, D.W., and Li, Y., 1994, Inversion of induced polarization data: Geophysics, **59**, 1327–1341.

Pelton, W.H., Ward, S.H., Hallof, P.G., Sill, W.R., and Nelson, P.H., 1978, Mineral discrimination and removal of inductive coupling with multi-frequency IP: Geophysics **43**, 588–609.

Revil, A., Abdel Aal, G.Z., Atekwana, E.A., Mao, D., and Florsch, N., 2015a, Induced polarization response of porous media with metallic particles—Part 2. Comparison with a broad database of experimental data: Geophysics, **80**, D539–D552.

Revil, A., Florsch, N., and Mao, D., 2015b, Induced polarization response of porous media with metallic particles—Part 1: A theory for disseminated semiconductors: Geophysics, **80**, D525–D538.

Sastry, R.G., and Tesfakiros, H.G., 2006, Neural network based interpretation algorithm for combined induced polarization and vertical electrical soundings of coastal zones: Journal of Environmental & Engineering Geophysics, **11**, 197–211.

Schmutz, M., Ghorbani, A., Vaudelet, P., and Revil, A., 2011, Spectral induced polarization detects cracks and distinguishes between open-and clay-filled fractures: Journal of Environmental and Engineering Geophysics, **16**, 85–91.

Sun, J., Li, Y., and Nabighian, M., 2012, Lithology differentiation based on inversion of full waveform induced polarization data from Newmont distributed IP data acquisition system (NEWDAS): *in* Expanded Abstracts: SEG Las Vegas 2012 Annual Meeting, Society of Exploration Geophysics.

Wang, W., Wu, X., and Spitzer, K., 2013, Three-dimensional DC anisotropic resistivity modelling using finite elements on unstructured grids: Geophysical Journal International, **193**, 734–746.

Winchen, T., Kemna A., Vereecken H., and Huisman J.A., 2009, Characterization of bimodal facies distributions using effective anisotropic complex resistivity: A 2D numerical study based on Cole-Cole models: Geophysics **74**, A19–A22.

Yin, C., 2000, Geoelectrical inversion for a one-dimensional anisotropic model and inherent non-uniqueness: Geophysical Journal International, **140**, 11–23.

Zhdanov, M.S., Gribenko, A., Burtman, V., and Dmitriev, V.I., 2008, Anisotropy of induced polarization in the context of the generalized effective-medium theory: *in* Expanded Abstracts: SEG Las Vegas 2008 Annual Meeting, Society of Exploration Geophysics.